Interaction of human neutrophil flavocytochrome *b* with cytosolic proteins: transferred-NOESY NMR studies of a gp91^{phox} C-terminal peptide bound to p47^{phox}

Earle R. ADAMS*, Edward A. DRATZ*, Dawit GIZACHEW*, Frank R. DeLEO†, Lixin YU†, Bryan D. VOLPP‡, Michael VLASES§, Algirdas J. JESAITIS§ and Mark T. QUINN†¶

†Department of Veterinary Molecular Biology, Montana State University, Bozeman, MT 59717, U.S.A., *Department of Chemistry and Biochemistry, Montana State University, Bozeman, MT 59717, U.S.A., §Department of Microbiology, Montana State University, Bozeman, MT 59717, U.S.A., and ‡Medical Service, West Palm Beach Veteran's Administration Medical Center, Palm Beach Garden, FL 33420, U.S.A.

During activation of the neutrophil NADPH oxidase, cytosolic p47^{phox} is translocated to the membrane where it associates with flavocytochrome *b* via multiple binding regions, including a site in the C-terminus of gp91^{phox}. To investigate this binding site further, we studied the three-dimensional structure of a gp91^{phox} C-terminal peptide (^{551}SNSESGPRGVHFIFNKEN^{568}) bound to p47^{phox} using transferred nuclear Overhauser effect spectroscopy (Tr-NOESY) NMR. Using MARDIGRAS analysis and simulated annealing, five similar sets of structures of the p47^{phox}-bound peptide were obtained, all containing an extended open bend from Ser^{5} to Phe^{14} (corresponding to gp91^{phox} residues 555–564). The ends of the peptide were poorly defined, however, suggesting they were more flexible. Therefore further refinement was performed on the Ser^{5}–Phe^{14} region of the peptide after omitting the ends of the peptide from consideration. In this case, two similar structures were obtained. Both structures again exhibited extended open-bend conformations. In addition, the amino acid side chains that showed evidence of immobilization on binding to p47^{phox} correlated directly with those that were found previously to be essential for biological activity. Thus during NADPH oxidase assembly, the C-terminus of gp91^{phox} binds to 47^{phox} in an extended conformation between gp91^{phox} residues 555 and 564, with immobilization of all of the amino acid side chains in the ^{558}RGVHFIF^{564} region except for His^{561}.

INTRODUCTION

Neutrophils play an essential role in the body's defence against pathogens [1]. On exposure to pathogenic stimuli, neutrophils respond by generating toxic oxygen species such as superoxide anion ($O_2^{-\cdot}$) and other potent microbiocidal agents [1]. The generation of these oxidants by neutrophils occurs through the activation of a membrane-associated complex known as the NADPH oxidase. In resting cells, the components of the NADPH oxidase are segregated into cytosolic and membrane compartments; however, the cytosolic components are translocated to the plasma membrane during activation and assemble with membrane-bound components, resulting in the active $O_2^{-\cdot}$-generating system (reviewed in [2,3]).

The key membrane-associated component of the NADPH oxidase is a heterodimeric flavocytochrome *b*, which is composed of a 91 kDa glycoprotein (gp91^{phox}) and a 22 kDa protein (p22^{phox}) (reviewed in [4,5]). Flavocytochrome *b* has been reported to contain all of the redox components of the NADPH oxidase [6–8] and is responsible for the direct transfer of electrons from NADPH to O_2. During activation of the neutrophil NADPH oxidase, p47^{phox} binds directly to flavocytochrome *b* [9–11], and at least six regions of flavocytochrome *b* have been identified as binding sites for p47^{phox} [9,12–17]. The first of these binding sites reported was identified by Kleinberg et al. [9,11], who found that synthetic peptides mimicking the C-terminus of gp91^{phox} inhibited $O_2^{-\cdot}$ generation in a cell-free NADPH oxidase assay system and in permeabilized cells. Furthermore the active gp91^{phox} peptides disrupted assembly of the NADPH oxidase complex by blocking the interaction between flavocytochrome *b* and p47^{phox}. Nakanishi et al. [12] subsequently confirmed these studies, and our recent analysis of p47^{phox} using random-sequence peptide phage-display mapping was consistent with the presence of a p47^{phox}-binding site on the C-terminus of gp91^{phox} [17]. Thus p47^{phox} binds to flavocytochrome *b* at multiple peptide domains on both subunits, including two or more sites on the C-terminus of gp91^{phox}, and synthetic peptides representing these domains on gp91^{phox} can compete with gp91^{phox} for binding to p47^{phox}.

Transferred nuclear Overhauser spectroscopy (Tr-NOESY) NMR has been used to study the structure of protein–protein contact interfaces by providing information on the bound structures of peptide sequences that block the interactions of interest [18–20]. In the present report, Tr-NOESY NMR techniques were used to study the conformation of a synthetic gp91^{phox} C-terminal mimetic peptide, ^{551}SNSESGPRGVHFIFNKEN^{568}, when it was bound to recombinant p47^{phox}. Our results show that this gp91^{phox} peptide binds to p47^{phox} in an extended open-bend conformation between Ser^{555} and Phe^{564}. These experiments also provide direct evidence supporting the immobilization of certain key amino acid side chains of the gp91^{phox} C-terminus during its interaction with p47^{phox}.

MATERIALS AND METHODS

Preparation and fractionation of neutrophils

Human neutrophils were isolated as described previously using dextran sedimentation followed by Histopaque density-gradient separation [21]. Membrane and cytosolic fractions were prepared by sequential centrifugation of cavitated neutrophils as described previously [17] and stored at −70 °C.

Abbreviations used: Tr-NOESY, transferred-nuclear Overhauser effect spectroscopy.

¶ To whom correspondence should be addressed.

Synthetic peptide

The gp91^{phox} peptide, ^{551}SNSESGPRGVHFIFNKEN^{568}, was synthesized on a Milligen 9050 peptide synthesizer and purified by preparative HPLC. Peptide preparations were found to have a mass of 2019 by electrospray MS, equal to the theoretical mass, and less than 2% contamination by species of other molecular masses was detected.

The synthetic gp91^{phox} C-terminal peptide was evaluated in a cell-free NADPH oxidase assay and in an electropermeabilized neutrophil system to confirm its biological activity. In the cell-free oxidase assay system [17], the peptide fully inhibited NADPH oxidase activity with an IC_{50} of approx. 50 μM (data not shown). This peptide also inhibited NADPH oxidase activity in electropermeabilized neutrophils at less than < 100 μM [22], confirming the cell-free assay results. These results are consistent with those of Kleinberg et al. [9,11] using similar peptides.

Production and purification of recombinant p47^{phox}

Recombinant p47^{phox} was produced in recombinant baculovirus-infected Sf9 cells and purified to homogeneity by the methods of Leto et al. [23]. The purity (> 99%) and identity of the recombinant p47^{phox} were confirmed by SDS/PAGE and Western blotting with anti-p47^{phox} antibodies [24]. In addition, the recombinant p47^{phox} was found to be active in reconstituting NADPH oxidase activity in a recombinant cell-free reconstitution system using neutrophil plasma membranes and recombinant cytosolic proteins [25], confirming that the recombinant p47^{phox} preparations were biologically active.

Preparation of NMR samples

Samples of gp91^{phox} C-terminal peptide were dissolved at 2.5 mM in 500 μl of 50 mM sodium phosphate, pH 6.5, containing 10% ^2H_2O and 0.75% 3-(trimethylsilyl)-[2,2,3,3-^{2}H]propionic acid (sodium salt) (TSP), and the pH was readjusted to 6.5. For NMR analysis of the bound peptide, 250 μl of 4.0 mM gp91^{phox} peptide (prepared in 50 mM sodium phosphate, pH 6.5, plus 0.75% TSP) was added dropwise to 200 μl of recombinant p47^{phox} (25 mg/ml in 50 mM sodium phosphate buffer, pH 6.5) with frequent adjustment of the pH to 6.5. ^2H_2O was added to bring the total volume to 500 μl, and final concentrations of peptide and p47^{phox} were 2.0 mM and 200 μM respectively. We noticed that some preparations of the peptide/protein mixture were initially fully soluble but tended to precipitate over time. Thus care was taken to ensure that samples used for NMR measurements had little or no precipitated material.

NMR spectroscopy

NMR spectra were measured on a Bruker AM 500 spectrometer using a proton-selective probe. TOCSY spectra [26] were collected at 1 °C with a MLEV-17 spin lock time of 100 ms. NOESY spectra [27] were collected at several temperatures, including 1 °C with mixing times of 75, 100, 125, 150, 200 and 300 ms. Mixing times were randomly varied over a range of ± 10% in order to reduce effects of zero-quantum coherence transfer [28]. All spectra were acquired with the RF carrier on the water resonance which was suppressed with coherent decoupler irradiation in the case of TOCSY or with jump and return read pulses in NOESY [29,30]. Residual water was further suppressed by a convolution function [31]. The transmitter phase and preacquisition delay were adjusted for NOESY spectra to eliminate the requirement for phase adjustment of the spectra during processing, which greatly improved baseline flatness [32]. For NOESY, the initial D0 delay in t_1 was adjusted to be equal to $IN/2 = 47.5$ μs minus an allowance of $4\tau/\pi$ for the finite lengths (τ) of the jump and return read pulses [33], and the phase in t_1 was set to PH0 = 45 and PH1 = -90, which resulted in greatly improved baseline flatness. NMR data were processed on Silicon Graphics workstations using FELIX (Hare Research Inc.) macros written at Montana State University by Christophe Lambert. Typically, 60°-shifted sine bell apodization functions were applied in t_2 and t_1 with zero filling to 2048 complex points. A 1/sin ($\Delta\omega$ D2) correction was applied to the NOESY intensity in F_2 to compensate for the non-uniform jump and return excitation, where $\Delta\omega$ is the offset from the water resonance and D2 is the delay between the jump and return pulses. This correction retrieved intensity losses due to jump and return detection, which are particularly important in the α proton region close to water (C. Lambert and E. A. Dratz, unpublished work).

Proton $T_{1\rho}$ relaxation experiments were carried out with the RF carrier set on the resonance of interest during spin lock and acquisition and then moved to the H_2O resonance during the relaxation delay where weak phase-coherent irradiation was used to suppress the solvent H_2O. Spin lock times were varied from 1 to 300 ms, and peak amplitudes were measured using a cubic spline-corrected baseline. $T_{1\rho}$ values were measured as a function of spin lock power from 200 to 21 000 Hz. Spin lock powers were directly calibrated by 180° pulse length measurements between 21 000 and 2400 Hz and calculated from the attenuator settings at lower powers. T_1 and T_2 relaxation experiments were carried out with inversion recovery and Carr–Purcell–Meiboom–Gill spin echo sequences, respectively with coherent presaturation for solvent suppression.

NOESY peak volumes were obtained using FELIX. T_1 values were found to be rather constant along the peptide spectrum in the presence of p47^{phox}. NOESY cross-peak intensities were divided by the volume of a resolved diagonal peak to correct for cross-peak intensity loss due to T_1 relaxation and to provide fractional NOESY intensities. The fractional NOESY intensities of the free peptide were subtracted from the observed fractional Tr-NOESY intensities in the presence of p47^{phox} to obtain the bound fractional NOESY intensities [see eqn. (1)]. This procedure assumes that the peptides are in fast exchange with their protein-binding sites on the cross-relaxation time scale, an assumption that was supported by the $T_{1\rho}$ measurements, as explained in the results. The bound fractional NOESY intensities at a mixing time of 200 ms were converted into approximate proton distances, using the isolated two-spin approximation and the side-chain amino protons of Asn (1.8 Å) as a reference intensity. Other proton pairs with known separation distances and resolved resonances such as Ile $\gamma_1 - \gamma_2$ were not stereospecifically assigned and were treated as pseudo-atoms in the MARDIGRAS refinements.

Molecular dynamics, simulated annealing and a variety of analysis routines in the Discover v2.8, InsightII v2.2, X-PLOR v3.1 and NMRchitect v2.0 packages (Biosym) were used in the structure analysis. Pseudo-atom corrections [34] were applied to the distance constraints involving methylene and methyl groups. All NOESY distance constraints were initially applied with force constants of 100 kcal/(mol·Å^2) and the force constants were manipulated in simulated annealing as described below. Chirality restraints were applied on all chiral atoms and omega angle restraints were applied with force constants of 300 kcal/(mol·rad^2) to maintain peptide bonds in the *trans* conformation. Families of ISPA structures obtained from simulated annealing were used as starting points for a MARDIGRAS [35] full relaxation matrix analysis to obtain improved distance constraints. Programs required for conversion of Biosym file formats to MARDIGRAS formats were written by David Poole in our laboratory.

RESULTS

^{1}H NMR spectra of the free gp91^{phox} carboxyl-tail peptide

The ^{1}H NMR spectra of the 18-amino acid gp91^{phox} C-terminal peptide (^{551}SNSESGPRGVHFIFNKEN^{568}) was assigned using a combination of two-dimensional TOCSY and NOESY NMR [36], and Table 1 shows the resonance assignments. Sequential assignments were readily accomplished from residues 2 to 18 with the aid of the sequential NH-αH and the NH-NH connectivity using the longer mixing time NOESYs. Most of the amide to α-cross-peaks within the same residue were resolved in the TOCSY NH-αH fingerprint region except for overlapping Ser^5 NH-αH and Phe^{14} NH-αH cross-peaks. The Asn^2 NH-αH cross-peak was not observed in TOCSY, but was seen in NOESY. The Ser^1 resonances were not identified because of the lack of an NH signal and partial overlap with Ser^3 and Ser^5.

NMR spectroscopy of the gp91^{phox} carboxyl-tail peptide bound to p47^{phox}

The central goal of the present experiments was to study the p47^{phox}-bound conformation of the gp91^{phox} carboxyl-tail peptide. To accomplish this goal, we performed Tr-NOESY measurements on the peptide in exchange with p47^{phox}, and Figure 1 shows contour plots of the fingerprint and aliphatic regions of the Tr-NOESY and free peptide NOESY spectra. These regions showed significant differences between the free- and bound-peptide spectra, while the amide region (not shown) only showed intensity differences between the two spectra. The resonance assignments of the peptide in exchange with the protein could be carried over from the free peptide since the relatively low fraction bound (~ 0.1) led to relatively small chemical-shift changes in the presence of p47^{phox}. The Tr-NOESY cross-relaxation rate observed for protons i and s on a ligand in fast exchange with a high-molecular-mass receptor is:

$$\sigma_{is}^{obs} = p_f \sigma_{is}^{f} + p_b \sigma_{is}^{b} \quad (1)$$

where p_f and p_b are the mole fractions and σ_{is}^{f} and σ_{is}^{b} are the cross-relaxation rates of the free and bound ligand respectively [37]. Although the free ligand is in large excess ($p_f \gg p_b$), the σ_{is}^{obs} can be dominated by the bound ligand cross-relaxation ($p_b \sigma_{is}^{b} \gg p_f \sigma_{is}^{f}$) in the Tr-NOESY because of the large increase in correlation time of the peptide when it is bound to a macromolecular receptor. Comparison of the peptide NOESY in the presence and absence of p47^{phox} ($\sim 10:1$ ratio of peptide/protein) indicated that the Tr-NOESY intensities were dominated by the bound ligand, as shown in part in Figure 1, while the chemical shift and appearance of the observed peptide NMR spectra are dominated by the excess free species.

In order for the simple form of eqn (1) to be valid, the peptide off-rate (k_{-1}) must be considerably faster than the fastest cross-relaxation rate of the ligand in the bound state (σ_{is}^{b}) [37]. Ligand off-rates were measured using $T_{1\rho}$ relaxation experiments as a function of the strength of the applied spin locking RF field (ω_{SL}) [38,39]. Davis et al. [39] showed that the $T_{1\rho}$ relaxation rate of a ligand in exchange between the free and bound states ($R_{1\rho}^{ex}$) can be described as a weighted sum of $1/T_1$ and $1/T_2$ in the bound and free states plus an exchange term as shown in their equation number 24. Crucial variables are $\Delta\omega$, which is the difference in chemical shift between the free and bound species; the off-rate $k_{ex} = (p_f)^{-1} k_{-1} \approx k_{-1}$; and $\Delta\omega_o$, the difference between the RF frequencies and the resonance frequency observed for the ligand when it is in exchange with the receptor. In the present experiments, $\Delta\omega_o = 0$ since the RF carrier was set on the observed resonance peak of the ligand of interest when it was in exchange with receptor and therefore, $\Delta\omega_o = 0$ and $\sin\beta = 1$ in equation 24 of Davis et al. [39].

Although most of the peptide resonances showed little chemical-shift difference due to binding to p47^{phox}, several resonance shifts were observed, and we investigated peaks that showed the largest shifts on binding to p47^{phox} for investigation by $T_{1\rho}$. The larger the $\Delta\omega$, the greater the difference in precession rate of the spin of interest between the bound and free states. When the dephasing due to $\Delta\omega$ approaches a rate similar to the k_{-1} process, there is a loss of spin lock and a faster decay in the amplitude of the detected magnetization. The Gly^6 αH and Asn^{15} NH side-chain proton resonances both exhibited easily detectable changes in chemical shift between the free and bound peptide. Because of uncertainties in the exact fraction of p47^{phox} that was able to bind peptide during the relaxation measurements, the fraction bound (p_b) and $\Delta\omega$ were varied along with k_{ex} to obtain the best fit to the data. The position of the inflection point in the $T_{1\rho}$ rate as a function of ω_{SL} is set primarily by the value of k_{ex} and indicated that the off-rate was approx. 1000 s^{-1}.

Mixing concentrated p47^{phox} with the peptide often caused precipitation of the sample at lower pH values (< 6.0), whereas higher pH values caused a loss in NH signal intensity due to proton exchange. Therefore the best compromise for maintaining NH signal intensity and solubility was found to be at pH 6.5, and, in samples where solubility was maintained, rather short Tr-NOESY spectra were run because of concerns that precipitation might occur. Therefore a relatively low number of scans and t_1 transients were used, and the Tr-NOESY measuring times were less than 8 h at each mixing time. These shorter measuring times, combined with the modest peptide concentration attainable, gave Tr-NOESY spectra with a modest signal-to-noise ratio. As

Table 1 Chemical shifts for the assigned ^{1}H resonances of the gp91^{phox} C-terminal peptide

Spectra were measured at 1 °C in 50 mM sodium phosphate, pH 6.5, as described in the Materials and methods section.

Residue	NH	αH	βH	Other protons
Asn^2	8.67	4.83	2.85, 2.90	γNH_2 7.11, 7.82
Glu^4	8.61	4.37	1.99, 2.13	γCH_2 2.28
Ser^5	8.48	4.52	3.90	
Gly^6	8.37	4.12		
Pro^7		4.40	2.01, 2.28	γCH_2 1.90
				δCH_2 3.64
Arg^8	8.72	4.35	1.78, 1.87	γCH_2 1.61, 1.66
				δCH_2 3.14
				NH 7.12, 7.28
Gly^9	8.52	3.96		
Val^{10}	8.16	4.03	1.97	γCH_3 0.80, 0.84
His^{11}	8.36	4.53	2.94	2H 8.14
				4H 7.11
Phe^{12}	8.65	4.71	3.06, 3.16	2, 6H 7.13
				3, 5H 7.15
Ile^{13}	8.14	4.07	1.69	γCH_2 1.08, 1.38
Phe^{14}	8.48	4.53	3.05	2, 6H 7.3
				3, 5H 7.36
Asn^{15}	8.5	4.63	2.66, 2.76	γNH_2 6.99, 7.72
Lys^{16}	8.42	4.24	1.77, 1.84	γCH_2 1.44
				δCH_2 1.7
				ϵCH_2 3.01
Glu^{17}	8.63	4.30	1.92, 2.10	γCH_2 2.28
Asn^{18}	8.18	4.44	2.69, 2.77	NH_2 6.93, 7.67

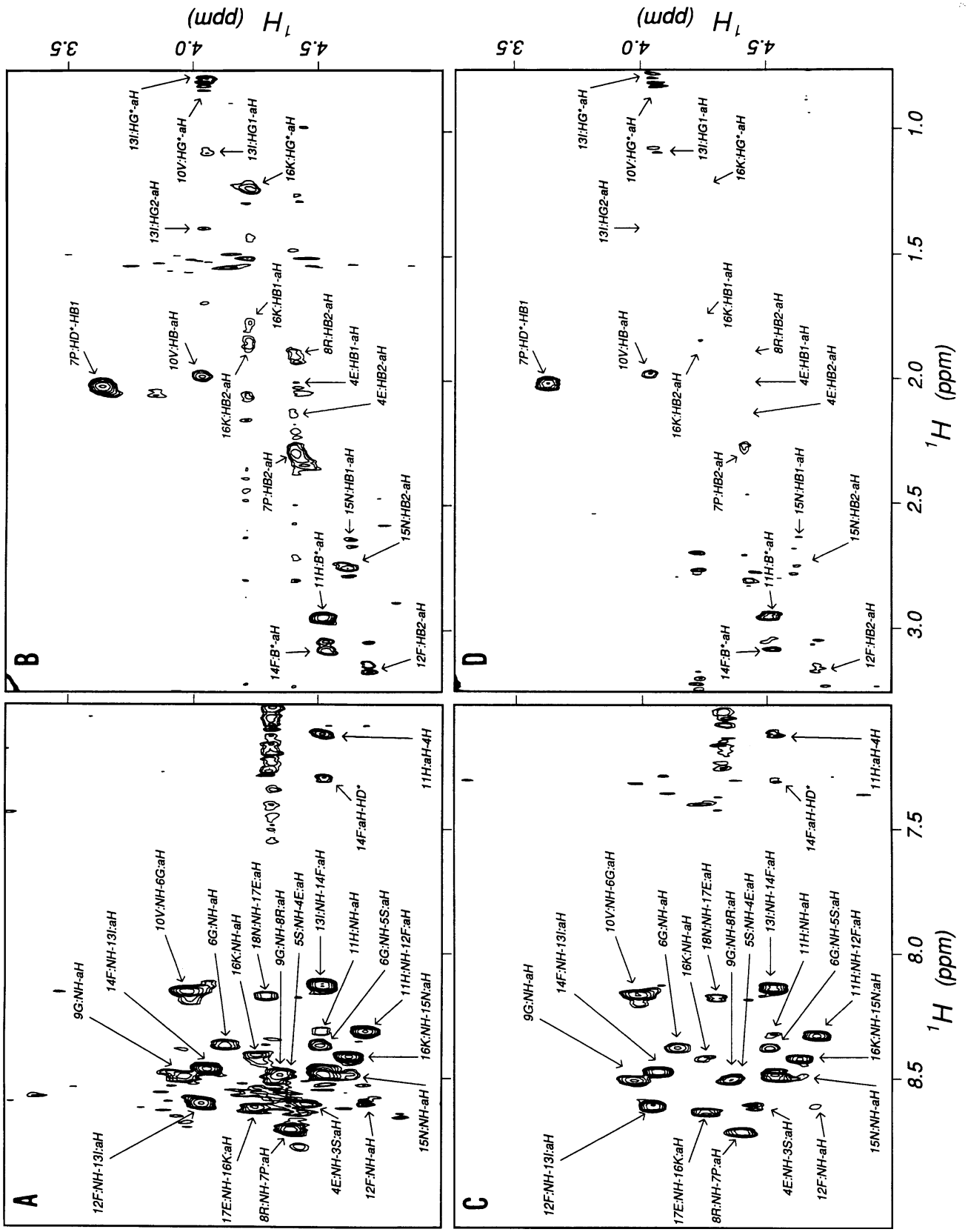

Figure 1 Contour plots of the fingerprint and aliphatic regions of the Tr-NOESY and NOESY NMR spectra

(**A**) and (**B**) Fingerprint and aliphatic regions respectively of the Tr-NOESY of 2 mM gp91^{phox} C-terminal peptide in the presence of 200 μM recombinant p47^{phox}. (**C**) and (**D**) Corresponding regions of the NOESY of 2.5 mM free gp91^{phox} C-terminal peptide. Assignments of many of the proton resonance cross-peaks are indicated.

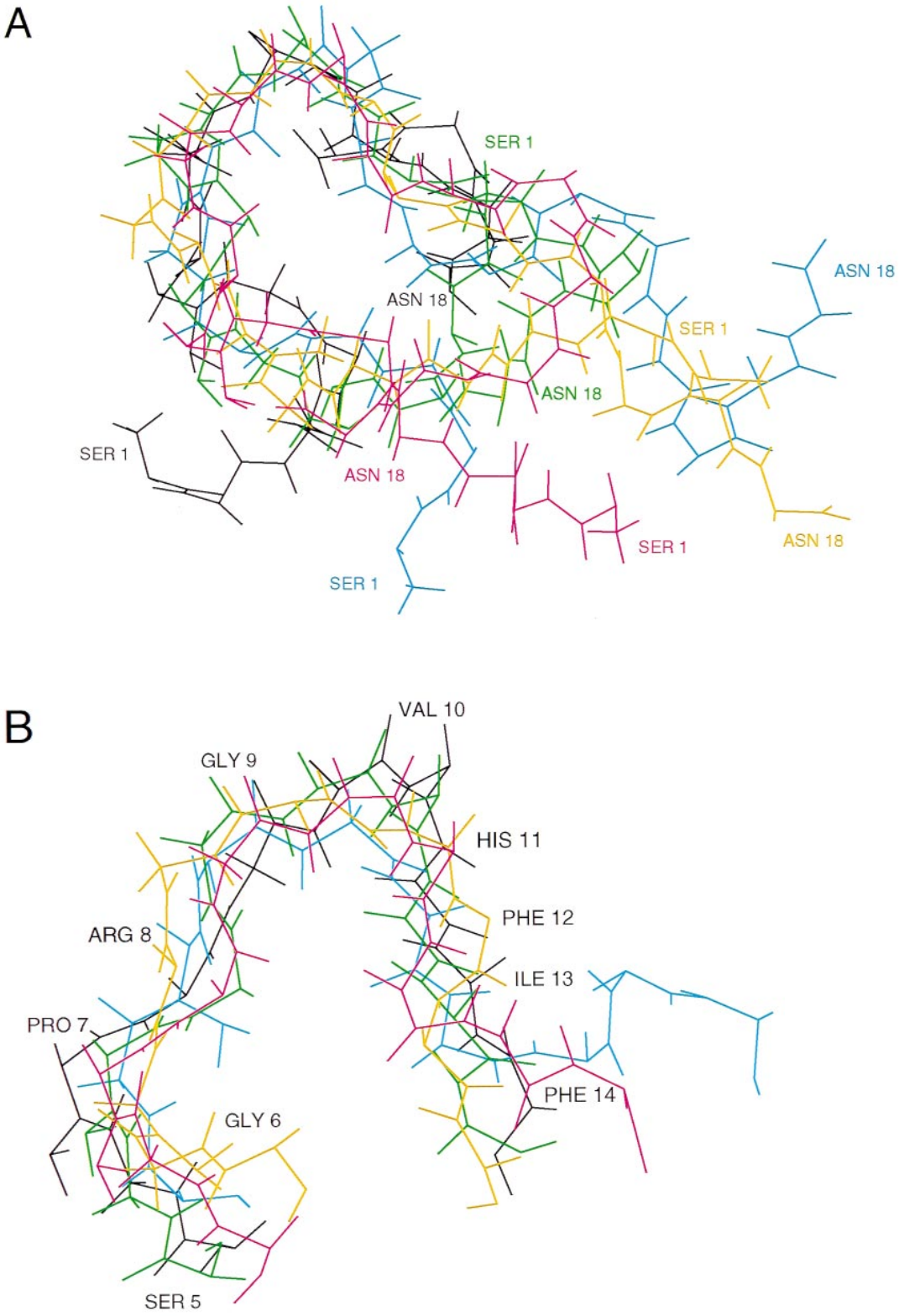

Figure 2 Superimposed MARDIGRAS-refined structures of the bound gp91^{phox} C-terminal peptide

The peptide backbone atoms of the lowest energy frames having the best agreement with the Tr-NOESY distance constraints after three cycles of refinement for each of the five clusters of structures were superimposed. (**A**) Entire peptide from Ser^{1} to Asn^{18} with each of the five structures shown in a different colour with the first and last residues of each peptide structure labelled in the same colour. (**B**) Peptide region from Ser^{5} to Phe^{14} superimposed for each structure shown in (**A**) with each amino acid residue in the peptide labelled.

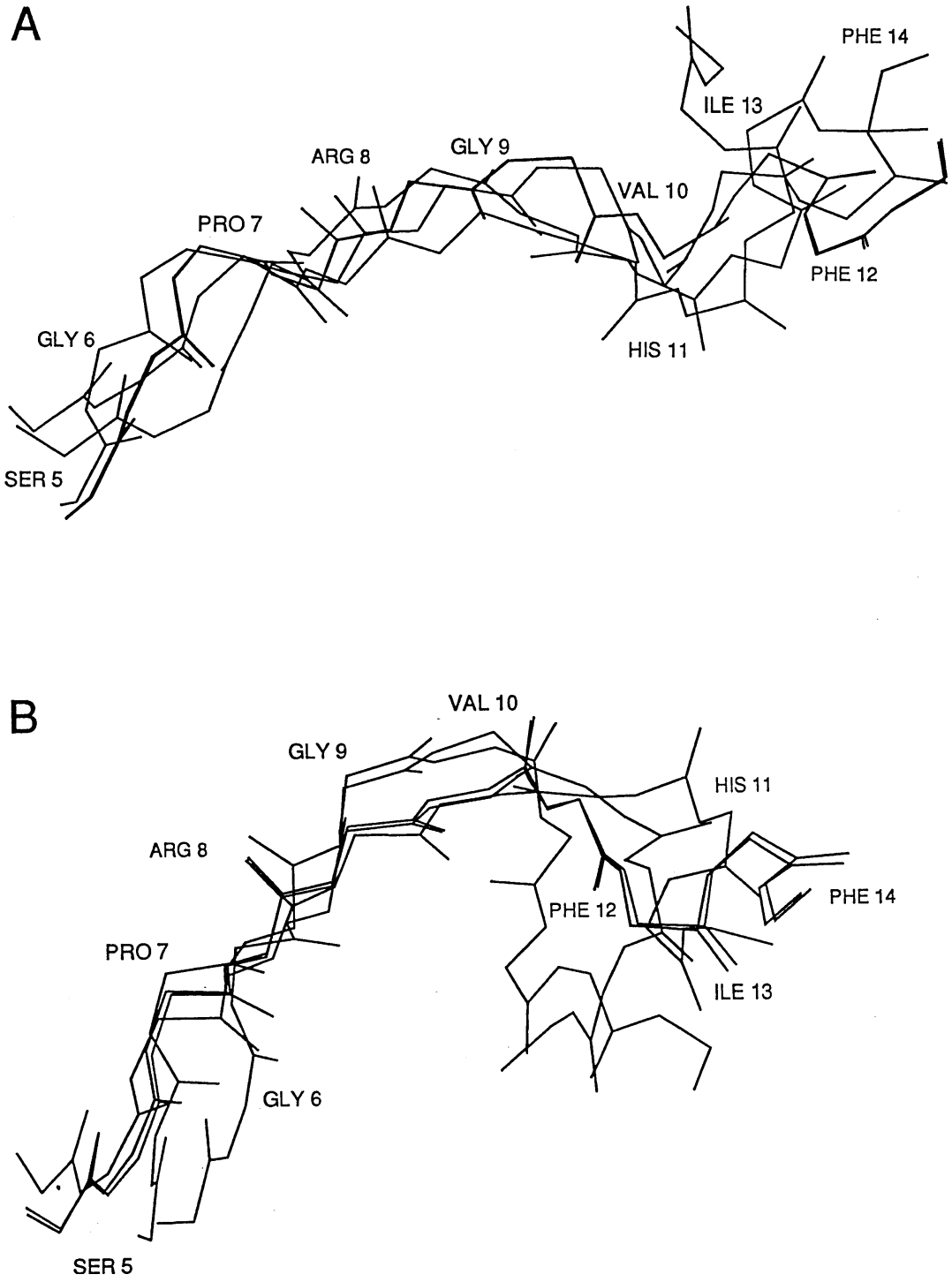

Figure 3 Superimposed MARDIGRAS-refined structures of the Ser[5]-Phe[14] region of the bound gp91^{phox} C-terminal peptide

The peptide backbone atoms of the two structures having the best agreement with the Tr-NOESY distance constraints after three cycles of refinement were superimposed.

shown in Figure 1, the addition of 0.2 mM p47^{phox} to 2 mM gp91^{phox} C-terminal peptide caused a large increase in many of the NOESY cross-peaks, while some of the cross-peaks decreased in intensity. Many cross-peak intensities in the aliphatic side-chain region increased significantly in the presence of p47^{phox}, especially in the region of Arg[8] to Lys[16]. A total of 126 Tr-NOESY cross-peaks was identified, which provided 98 i,i and 28 i,i-1 distance constraints. Long-range Tr-NOESY cross-peaks were not detected, suggesting that the peptide was in an extended conformation when bound to p47^{phox}.

Initial distance constraints (derived from the isolated two-spin approximation) were taken from the bound peptide Tr-NOESY intensities that had been corrected for free peptide contributions and T_1 relaxation as described in the Materials and methods

section. Tr-NOESY distance constraints, *trans*-peptide ω dihedral constraints, and chirality restraints were used in simulated annealing [40] to generate 20 trial structures. From these 20 structures, five structures were picked which had the lowest relative energies and best distance agreements. These five structures were then used as starting points for an iterative full relaxation matrix MARDIGRAS distance-refinement procedure [35].

MARDIGRAS-generated distance constraints are sensitive to the effective correlation time (τ_c^{eff}) of the ligand. When the ligand is bound to the receptor, it is expected to have a correlation time approaching that of the receptor. Therefore τ_c^{eff} of the gp91^{phox} C-terminal peptide in fast exchange represents a weighted average of the bound and free correlation times. The approximate correlation time of p47^{phox} is 24 ns using the Stokes–Einstein equation, which assumes a compact spherical shape for the protein. At a fraction bound (p_b) of 0.1, the effective τ_c of the peptide would be $\sim$ 2.4 ns. If a portion of the p47^{phox} in the preparation was not available to bind peptide because of misfolding and/or non-specific aggregation or if the bound peptide experienced more local motion than the whole protein, τ_c^{eff} could be lower. In addition, p47^{phox} could also have a longer correlation time than an equivalent sphere. Therefore τ_c^{eff} values slightly above and considerably below 2.4 ns (0.6, 0.8, 1.0, 2.0 and 3.0 ns) were used in MARDIGRAS refinements for each of the trial structures. The three lowest τ_c^{eff} values (0.6, 0.8 and 1.0 ns) gave the best Q and R values, which are measures of internal agreement with the data in the MARDIGRAS distance refinements [41]. Alternatively, the effective mixing time for the bound species was taken to be p_b times the experimental mixing time (e.g. 0.1×200 ms = 20 ms) [42]. In this case, the bound cross-relaxation rates are 10-fold larger ($1/p_b$) and a range of bound τ_c values was used (10, 12, 14, 16, 18, 20, 24, 30 ns) in MARDIGRAS. The best Q and R values were found at bound τ_c values of 14 and 16 ns with very similar best-fit distances.

Molecular dynamics was run using the MARDIGRAS distances from the three lowest correlation times as restraints and using the five starting structures derived from the prior round of simulated annealing as starting points, to generate 15 new sets of structures. The structures were analysed for RMS distance agreement, ω dihedral violations, and relative energy; a best structure was selected from each set. The 15 structures were then each subjected to another round of MARDIGRAS refinement. The MARDIGRAS refinement gave the best Q and R agreement with the data at an effective τ_c of 1.0 ns. The resulting 15 sets of MARDIGRAS distances were used in constrained molecular dynamics, and these runs were analysed for RMS distance agreements and relative energies. The structure refinement was iterated again with a third round of MARDIGRAS. The structures obtained with a τ_c of 1.0 ns had fewer distance violations than the structures obtained with either slower or longer correlation times. The Q and R factors and the MARDIGRAS distances were very similar in the second and third rounds of refinement, and therefore it was concluded that further refinement would produce no further improvement.

Five clusters of structures of the bound gp91^{phox} C-terminal peptide had the best internal agreement, lowest energy and lowest restraint violations, but none of the five sets was clearly preferred by the combination of these criteria (Figure 2A). However, all sets of structures had an extended open bend in the region of Ser^5 to Phe^{14}, while the bound structure was poorly defined outside of the Ser^5–Phe^{14} region (Figure 2A). Superimposition of the backbone atoms from residues Ser^5 to Phe^{14} using the lowest energy frame from each of the five structure clusters indicated that the bound structure of the peptide between Ser^5 and Phe^{14} was indeed very similar in all of these structures (Figure 2B).

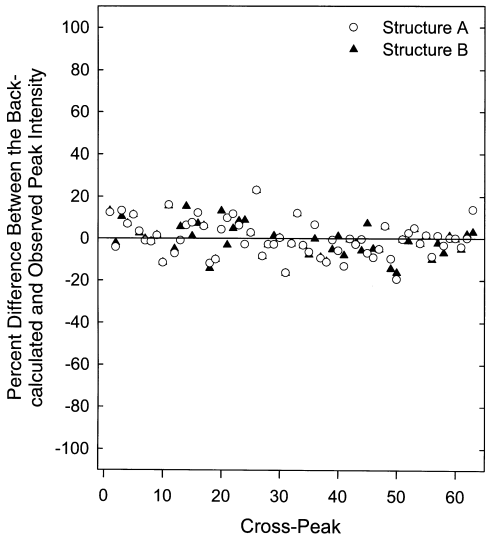

Figure 4 Comparison of the observed and back-calculated cross-peak intensities for each of the refined structures shown in Figure 3

The percentage difference between the back-calculated and experimentally observed intensity was calculated for each cross-peak using the following equation:
[(Back-calculated intensity — observed intensity)/observed intensity] $\times$ 100.

Table 2 Comparison of NOESY intensities between protons within amino acid side chains of the free and p47^{phox} -bound gp91^{phox} peptide

Bound intensities were obtained by subtracting the free intensities from the intensities observed in the presence of p47^{phox} and dividing the result by the fraction bound, which was assumed to be 0.1. In the event that the fraction bound was lower, the bound NOESY intensities would be even larger.

Amino acid residue and position in peptide	$10^6 \times$ Peak intensity	
	Free peptide	Bound peptide
Glu^4	1.94	38.60
Pro^7	0.11	46.10
Arg^8	0.25	3.20
Gly^9	—	—
Val^{10}	0.52	12.50
His^{11}	1.00	1.40
Phe^{12}	1.63	10.30
Ile^{13}	0.93	13.70
Phe^{14}	1.31	18.00
Asn^{15}	2.94	26.00
Lys^{16}	0.36	8.38

As shown in Figure 2, the conformation of the residues from Ser^1–Ser^3 and Lys^{15}–Asn^{18} was poorly defined by the data. Therefore these residues were removed from structural consideration, the co-ordinates of the best structures from Ser^5–Phe^{14} were randomized, and several rounds of simulated annealing and MARDIGRAS analysis were performed. This refinement resulted in two similar sets of structures that also exhibited extended or somewhat open-bend conformations (Figure 3). To confirm that these structures accurately represented our experimental data, we back-calculated the spectrum for each refined structure and found that the majority of back-calculated cross-peak intensities

were very similar to the experimental cross-peak intensities (Figure 4). Larger deviations ($\sim 20\,\%$ difference) occurred only for those cross-peaks that had unresolved proton peaks. Both sets of refined structures also had very low NOE violations; only four cross-peaks had NOE violations > 0.5 Å, and the maximum distance violation for any one cross-peak did not exceed 0.7 Å. These results indicate a good agreement between the calculated and experimentally observed data. The small NOE violations observed probably resulted from uncertainties in the NOE intensity measurements and/or the presence of local motion.

Certain amino acid side chains showed large increases in Tr-NOESY intensities in the presence of $p47^{phox}$ relative to the free peptide NOESYs (Figure 1 and Table 2), indicating that these particular side chains are significantly immobilized when the peptide binds to $p47^{phox}$. As summarized in Table 2, our data show that the amino acid side chains between residues 8 and 16 of the peptide, except for His^{11}, appear to interact strongly with $p47^{phox}$. The Gly^{9} protons did not show detectable splitting, and therefore a Tr-NOESY cross-peak could not be observed between them.

DISCUSSION

Previous studies have demonstrated that $gp91^{phox}$ C-terminal peptides can block assembly of the neutrophil NADPH oxidase by disrupting the interaction between flavocytochrome *b* and the $p47^{phox}$ protein [9,11,12]. In the present studies, we extend these observations to: (1) provide direct evidence supporting this binding interaction, (2) define the regions of intimate contact between the $gp91^{phox}$ C-terminal peptide and $p47^{phox}$, and (3) obtain information on the three-dimensional conformation of the peptide when it is bound to $p47^{phox}$.

In the presence of $p47^{phox}$, many Tr-NOESY cross-peaks of the $gp91^{phox}$ C-terminal peptide showed significant increases in intensity compared with those observed for the free peptide (see Figure 1 and Table 2). The increases in cross-peak intensities indicate substantial immobilization of many of the amino acid side chains in the peptide via interaction with $p47^{phox}$. The Tr-NOESY cross-peaks of the bound $gp91^{phox}$ C-terminal peptide did not show long-range intramolecular interactions, suggesting an extended conformation of this peptide when bound to $p47^{phox}$, and the peptide backbone structures shown in Figures 2 and 3 are consistent with this conclusion. The $gp91^{phox}$ C-terminal peptide bound to $p47^{phox}$ contains an extended open bend between Ser^{5} and Phe^{14} with close association of most of the amino acid side chains with $p47^{phox}$ (except His^{11}) and a poorly defined structure outside of this central region. This type of extended conformation is not inconsistent with the biochemical function of this binding site which contributes to a high-affinity multisite binding interaction that occurs between $p47^{phox}$ and $gp91^{phox}$ [9,12–17].

Peptide ligands have been shown to bind to target proteins in extended or open conformations in a number of systems studied with Tr-NOESY or X-ray diffraction, including a hexapeptide substrate bound to porcine pancreatic elastase [43], a dodecapeptide of the nicotinic acetylcholine receptor bound to α-bungarotoxin [44], a platelet receptor peptide bound to bovine α-thrombin [45] and endogenous peptides bound to the MHC I [46] and MHC II proteins [47]. In addition, other types of structure have been found for peptide ligands when bound to target proteins, including α-helices [19] and more complex shapes [20].

Using alanine substitution on similar peptides to the peptide studied here, Kleinberg et al. [11] reported that the residues corresponding to Arg^{8}, Val^{10}, Phe^{12}, Ile^{13} and Phe^{14} of the peptide we studied were all essential for inhibitory activity in NADPH oxidase assays. Substitution of alanine for Gly^{9} or His^{11} had little effect on the inhibitory activity of these peptides. In addition, extensions of the peptide on either end of this Arg^{8}–Phe^{14} region did not increase activity. Our results are consistent with these previous biochemical data and now show directly that the biologically active residues are those residues that also experience the strongest immobilization when interacting with $p47^{phox}$ (Table 2). Since some neighbouring residues outside of the minimal region conferring activity (Arg^{8}–Phe^{14}) also showed significant chemical shifts when bound to $p47^{phox}$, our data suggest that these peptide regions may contribute in some way to binding of the peptide to $p47^{phox}$, although they do not seem to confer further inhibitory activity on the peptide. In any case, the direct correlation between the changes in Tr-NOESY cross-peak intensities determined here and the peptide amino acid sequence requirements for biological activity determined previously by Kleinberg et al. [11] are consistent with each other.

A number of potential problems can arise in interpreting Tr-NOESY data, including viscosity artifacts and influences of spin diffusion between the ligand and its protein-binding site. In these experiments, we did not observe significant broadening of ligand signals in the presence of $p47^{phox}$, indicating that viscosity did not significantly contribute to the changes we observed in Tr-NOESY cross-peak intensities [48]. As described above in the Materials and Methods and Results sections, the exchange rate of the $gp91^{phox}$ C-terminal peptide appears to be sufficiently fast, relative to the cross-relaxation between protons on the bound peptide, to be interpreted in the fast-exchange limit for Tr-NOESY. In the fast-exchange region, the effective mixing time in Tr-NOESY is equivalent to the experimental mixing time (up to 300 ms in our experiments) multiplied by the fraction of ligand bound ($\leqslant 0.1$ in the present experiments) [42,49]. Thus the spin diffusion to the protein would be effective for 30 ms or less in our experiments, assuming all of the protein bound peptide and for approx. 15 ms if only half of the $p47^{phox}$ was folded correctly or accessible to bind ligand (lower limit). Such short effective mixing times tend to reduce the influence of spin diffusion while the peptide is bound. In addition, intramolecular spin diffusion can be largely accounted for by complete relaxation matrix analysis, as was done here using MARDIGRAS [50].

Tr-NOESY NMR analysis of peptide ligands bound to protein receptors appears to be a useful approach to obtain structural information on regions of protein–protein interactions. The phagocyte NADPH oxidase is a multicomponent enzyme complex, the assembly of which involves the interaction of at least six different protein components and therefore many sites of protein–protein contact. The present studies provide a starting point to define the structural nature of this assembly and provide a basis for the further understanding of how the activation of the oxidase is regulated at the molecular level. In addition, this type of structural information might eventually be used to guide the synthesis of non-peptide mimetic compounds with higher affinity that would have potential therapeutic usefulness in treating inflammatory diseases.

This work was supported in part by National Institutes of Health FIRST Award AR40929 (to M.T.Q.), RO1 AR42426 (to M.T.Q.) and RO1 AI26711 (to A.J.J.), an Arthritis Foundation Biomedical Science Grant (to M.T.Q.), and a National Science Foundation EPSCoR grant RII-891878 (to E.A.D.). M.T.Q. is an Established Investigator of the American Heart Association. This is article no. J-4008 from the Montana State University Agricultural Experimental Station.

REFERENCES

1 Baggiolini, M., Boulay, F., Badwey, J. A. and Curnutte, J. T. (1993) FASEB J. **7**, 1004–1010

2 Robinson, J. M. and Badwey, J. A. (1995) Histochemistry **103**, 163–180
3 DeLeo, F. R. and Quinn, M. T. (1996) J. Leukoc. Biol. **60**, 677–691
4 Segal, A. W. (1989) J. Clin. Invest. **83**, 1785–1793
5 Jesaitis, A. J. (1995) J. Immunol. **155**, 3286–3288
6 Rotrosen, D., Yeung, C. L., Leto, T. L., Malech, H. L. and Kwong, C. H. (1992) Science **256**, 1459–1462
7 Segal, A. W., West, I., Wientjes, F., Nugent, J. H. A., Chavan, A. J., Haley, B., Garcia, R. C., Rosen, H. and Scarce, G. (1992) Biochem. J. **284**, 781–788
8 Koshkin, V. and Pick, E. (1993) FEBS Lett. **327**, 57–62
9 Kleinberg, M. E., Malech, H. L. and Rotrosen, D. (1990) J. Biol. Chem. **265**, 15577–15583
10 Heyworth, P. G., Curnutte, J. T., Nauseef, W. M., Volpp, B. D., Pearson, D. W., Rosen, H. and Clark, R. A. (1991) J. Clin. Invest. **87**, 352–356
11 Kleinberg, M. E., Mital, D., Rotrosen, D. and Malech, H. L. (1992) Biochemistry **31**, 2686–2690
12 Nakanishi, A., Imajohohmi, S., Fujinawa, T., Kikuchi, H. and Kanegasaki, S. (1992) J. Biol. Chem. **267**, 19072–19074
13 Leusen, J. H. W., De Boer, M., Bolscher, B. G. J. M., Hilarius, P. M., Weening, R. S., Ochs, H. D., Roos, D. and Verhoeven, A. J. (1994) J. Clin. Invest. **93**, 2120–2126
14 Leusen, J. H. W., Bolscher, B. G. J. M., Hilarius, P. M., Weening, R. S., Kaulfersch, W., Seger, R. A., Roos, D. and Verhoeven, A. J. (1994) J. Exp. Med. **180**, 2329–2334
15 Sumimoto, H., Kage, Y., Nunoi, H., Sasaki, H., Nose, T., Fukumaki, Y., Ohno, M., Minakami, S. and Takeshige, K. (1994) Proc. Natl. Acad. Sci. U.S.A. **91**, 5345–5349
16 Leto, T. L., Adams, A. G. and de Mendez, I. (1994) Proc. Natl. Acad. Sci. U.S.A. **91**, 10650–10654
17 DeLeo, F. R., Yu, L., Burritt, J. B., Loetterle, L. R., Bond, C. W., Jesaitis, A. J. and Quinn, M. T. (1995) Proc. Natl. Acad. Sci. U.S.A. **92**, 7110–7114
18 Campbell, A. P. and Sykes, B. D. (1991) J. Magn. Reson. **93**, 77–92
19 Campbell, A. P. and Sykes, B. D. (1991) J. Mol. Biol. **222**, 405–421
20 Dratz, E. A., Furstenau, J. E., Lambert, C. G., Thireault, D. L., Rarick, H., Schepers, T., Pakhlevaniants, S. and Hamm, H. E. (1993) Nature (London) **363**, 276–281
21 Quinn, M. T., Parkos, C. A. and Jesaitis, A. J. (1989) Biochim. Biophys. Acta **987**, 83–94
22 DeLeo, F. R., Jutila, M. A. and Quinn, M. T. (1996) J. Immunol. Methods **198**, 35–49
23 Leto, T. L., Garrett, M. C., Fujii, H. and Nunoi, H. (1991) J. Biol. Chem. **266**, 19812–19818
24 DeLeo, F. R., Nauseef, W. M., Jesaitis, A. J., Burritt, J. B., Clark, R. A. and Quinn, M. T. (1995) J. Biol. Chem. **270**, 26246–26251
25 DeLeo, F. R., Ulman, K. V., Davis, A. R., Jutila, K. L. and Quinn, M. T. (1996) J. Biol. Chem. **271**, 17013–17020
26 Bax, A. and Davis, D. (1985) J. Magn. Reson. **65**, 355–360
27 Jeener, J., Meier, B. H., Bachman, P. and Ernst, R. R. (1979) J. Chem. Phys. **71**, 4546–4553
28 Macura, S., Huang, Y., Suter, D. and Ernst, R. R. (1981) J. Magn. Reson. **43**, 259–281
29 Plateau, P. and Gueron, M. (1982) J. Am. Chem. Soc. **104**, 7310–7311
30 Driscoll, P. C., Clore, G. M., Beress, L. and Gronenborn, A. M. (1989) Biochemistry **28**, 2178–2187
31 Marion, D., Ikura, M. and Bax, A. (1989) J. Magn. Reson. **84**, 425–430
32 Marion, D. and Bax, A. (1988) J. Magn. Reson. **79**, 352–356
33 Bax, A., Ikura, M., Kay, L. E. and Zhu, G. (1991) J. Magn. Reson. **91**, 174–178
34 Wuthrich, K., Billeter, M. and Braun, W. (1983) J. Mol. Biol. **169**, 949–961
35 Borgias, B. A. and James, T. L. (1990) J. Magn. Reson. **87**, 475–487
36 Wuthrich, K. (1986) NMR of Proteins and Nucleic Acids, John Wiley & Sons, New York
37 Clore, G. M. and Gronenborn, A. M. (1982) J. Magn. Reson. **48**, 402–417
38 Stilbs, P. and Moseley, M. E. (1978) J. Magn. Reson. **31**, 55–61
39 Davis, D. G., Perlman, M. E. and London, R. E. (1994) J. Magn. Reson. **104**, 266–275
40 Nilges, M., Clore, G. M. and Gronenborn, A. M. (1988) FEBS Lett. **239**, 25–42
41 Withka, J. M., Srinivasa, J. and Bolton, P. H. (1992) J. Magn. Reson. **98**, 611–617
42 Landy, S. B. and Rao, B. D. N. (1989) J. Magn. Reson. **81**, 371–377
43 Meyer, E. F., Clore, G. M., Gronenborn, A. M. and Hansen, H. A. (1988) Biochemistry **27**, 725–730
44 Basus, V. J., Song, G. and Hawrot, E. (1993) Biochemistry **32**, 12290–12298
45 Ni, F., Ripoll, D. R., Martin, P. D. and Edwards, B. F. P. (1992) Biochemistry **31**, 11551–11557
46 Bjorkman, P. J. (1989) J. Mol. Biol. **206**, 677–689
47 Brown, J. H., Jardetzky, T. S., Gorga, J. C., Stern, L. J., Urban, R. G., Strominger, J. L. and Wiley, D. C. (1993) Nature (London) **364**, 33–39
48 Amodeo, P., Motta, A., Picone, D., Saviano, G., Rancredi, T. and Temussi, P. A. (1991) J. Magn. Reson. **95**, 201–207
49 Lippens, G. M. and Hallenga, J. K. (1990) J. Magn. Reson. **88**, 619–626
50 Davis, J. H., Bradley, E. K., Miljanich, G. P., Laszlo, N. and Ramachandran, J. (1993) Biochemistry **32**, 7396–7405

Received 18 November 1996/20 February 1997; accepted 6 March 1997